# SEGMENTATION OF WHEAT GRAINS IN THERMAL IMAGES BASED ON PULSE COUPLED NEURAL NETWORKS

*Mario Chacon*[1], *Annamalai Manickavasagan*[2], *Daniel Flores-Tapia*[3], *Gabriel Thomas*[3], *Digvir S. Jayas*[2]

[1]DSP & Vision Laboratory, Chihuahua Institute of Technology, Mexico
[2]Department of Biosystems Engineering, University of Manitoba, Canada
[3]Department of Electrical and Computer Engineering, University of Manitoba, Canada

## ABSTRACT

Canada is one of the major exporters of wheat in the world. The quality of these exports is well known and factors such as lack of insect infestation are very important. The use of thermal images for subsequent analysis of temperatures profiles for grain classification and insect detection is a method under investigation. This paper presents an approach for automatic image segmentation of the wheat kernels based on the combined use of wavelet analysis and pulse coupled neural networks. It is shown that using wavelets as a preprocessing technique yields a consistent accurate segmentation in terms of the iteration number in which the network yields reliable edges of the wheat kernels. Subsequent analysis of these segmentations can determine internal qualities such as infestations.

***Index Terms***— Static wavelet transform, pulse coupled neural network, grain segmentation, thermal images

## 1. INTRODUCTION AND MOTIVATION

Canada produces around 57Mt of grains every year and about 46% of that is exported. Wheat is the major grain in Canada and the annual production is about 43% (24.5 Mt) of the total grain production. To minimize losses by stored-product insects, early detection of infestations is required to carry out control measures. Knowledge on heating behavior and quality changes during drying using different methods such as microwave heating are essential to develop alternative grain drying systems. Similarly, in grain handling facilities, quick, reliable machine vision methods using visible and invisible imaging techniques are needed to assist grain inspectors in the determination of grain grading factors [1,2].

Thermal imaging is a method in which the invisible radiation pattern of an object is converted into a visible image. By this method, the surface temperature of any object can be mapped at a high resolution in two dimensions. The region in the infrared band with wavelengths from 3 to 14 μm is called the thermal infrared region. This band is useful in imaging applications that use heat signatures [3]. This technique has been used for several applications such as medical diagnostics, building inspection and quality evaluation of food materials. The quality evaluation of materials using thermal imaging involves two types of approaches: (i) induced state imaging, and (ii) steady state imaging. In the first approach, the object is heated and cooled by an external heating or cooling source, then thermal images of the objects are taken and analyzed. In this case, the object will be at a different temperature (hot or cold) from the background and therefore the image will be very clear and sharp. But in the second approach (steady state imaging), thermal images are taken without any treatment to the objects. At normal conditions, biological materials reach thermal equilibrium with the ambient conditions in a short time. Therefore thermal images of the biological materials taken at steady state usually have poor contrast. In some situations, the edges or boundary of the object are not clear. Furthermore, in some locations on the objects, the object color (temperature) is similar to the background. In this case, it is a challenging task to segment the object from the background in order to obtain useful features from the object. Regular thresholding techniques yielded poor segmentations in the steady state thermal images under consideration in this work. Hence the objective of this study was to develop an algorithm to segment accurately the wheat kernel from the background in steady state thermal images using an alternative method. After segmentation, the temperature profiles on the surface of the grain can be analyzed to determine internal qualities such as infestations.

## 2. IMAGE PREPROCESSING

An un-cooled focal planar array type infrared thermal camera (Model: ThermaCAM ™ SC500 of FLIR systems, Burlington, ON, Canada; spectral range: 7.5 to 13.0 μm), with 320×240 pixels, was used in this study. A 50 μm infrared close-up lens was attached to the original lens of the camera to obtain magnified thermal images of individual wheat kernels.

An image of a Canada western red spring wheat grain at 14% moisture content and its histogram are shown in

Figure 1. Note how the temperature sensitivity of the system yield images with not a lot of contrast and very specific gray level values. The original pixel intensities for this image vary from 303.3974 to 302.5749. A linear normalization was used in order to have a pixel intensity range from 0 to 255.

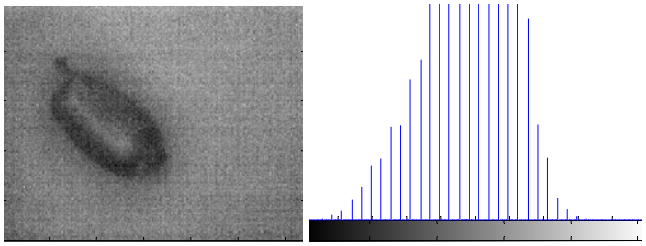

Figure 1. Left: Original image. Right: Histogram

Defining a fixed threshold to segment the grain from the background for this image is not a feasible task. A histogram in this scenario must resemble a bimodal distribution with a well defined valley [3] so that a histogram-based
thresholding algorithm can be used [4]. Therefore, a preprocessing step based on the use of the Static Wavelet Transform (SWT) was initially considered by the authors and is explained next.

The wavelet transform of a signal $f(x)$ is defined as [5]:

$$W_s(x) = f(x) \otimes \psi_s(x), \tag{1}$$

where $\psi$ is an orthogonal wavelet, $s$ is the scale of the wavelet function and $\otimes$ denotes convolution.

In [5], a different approach was proposed to obtain $W_s(x)$. Let us consider the wavelet packet to be composed by the wavelet $\psi$ and the scaling function $\theta$. The Discrete Wavelet Transform (DWT) algorithm states that the approximate form $A$ and the details $D$ from a signal $g$ are given by the following relation:

$$\begin{aligned} A_{i+1}(x) &= \langle g_i, \theta_{i+1}(x) \rangle \\ D_{i+1}(x) &= \langle g_i, \psi_{i+1}(x) \rangle \end{aligned}, \tag{2}$$

where $\langle \cdot, \cdot \rangle$ denotes the inner product, $g_i$ is the projection of $g$ at the $i^{th}$ level and $g_0=g$. In order to obtain the next level representations for the next decomposition level, the dual basis functions are expressed at a coarser level as dual scaling functions at the finer resolution level as indicated by:

$$\begin{aligned} \theta_s\left(\frac{x}{2}\right) &= \sum_{k=-\infty}^{\infty} w(k)\theta_s(x-k) \\ \psi_s\left(\frac{x}{2}\right) &= \sum_{k=-\infty}^{\infty} \hat{w}(k)\theta_s(x-k) \end{aligned}. \tag{3}$$

Here, $w(k)$ and $\hat{w}(k)$ are defined as the impulse response of a lowpass and a highpass Quadrature Mirror Filter (QMF), respectively. The length of the resulting products of the QMF and $g_s$ is twice the length of the input signal [5]. Therefore, the DWT basic computational step is a convolution followed by decimation. The decimation retains the even or the odd indexed elements and makes the DWT to be a time variant transform. In order to maintain the time invariance, the SWT does not perform the downsampling, giving as a result a time invariant wavelet analysis packet and a preprocessed image of the original size. This is an important feature since we would like to have a binary mask from the segmentation that can extract the pixels that are located within the grain in the original image that has the temperature information.

The stationary wavelet decomposition of the image shown in Figure 1 was computed and a blurred image as shown in Figure 2 was obtained using the coefficients of approximation of level 4 and a Daubechies wavelet. Albeit the histogram does not show a clear bimodal distribution and thresholding was not effective, segmentation of this blurred image was presumed to be an easier task at this point as it will be seen in the following sections.

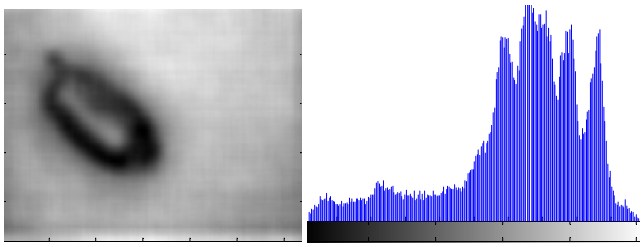

Figure 2. Left: Preprocessed image. Right: Histogram.

## 3. SEGMENTATION USING A PCNN

Segmentation of images using a Pulse Coupled Neural Network (PCNN) can be achieved even for cases in which images present overlap in the intensity ranges [6] such as the ones shown in the histograms of Figures 1 and 2. Recently, the use of a PCNN for image segmentation and classification of synthetic aperture radar images of sea ice has been proposed [7]. These radar images are notorious for having histograms that do not show well defined modes as discussed in the previous section.

Usually a PCNN is used as a preprocessing step in image processing as implemented in [8] for image segmentation purposes. PCNNs can also be used for image shadow removal [9], image fusion [10] and PCNNs applied to image processing is still an active area of research. This paper uses the PCNN processor proposed in [11] which is briefly described next.

The feeding region of the neural element of the PCNN can be described as

$$F(t) = G_{Feed} e^{-\alpha F \Delta t} F(t-1) + S + Y(t-1) * W \quad (4)$$

where $G_{Feed}$ is the feed gain, $S$ is input image, $\alpha_{F\Delta t}$ is the time constant of the likage filter of the feeding region, $Y(t)$ is the neuron output at time $t$, and $W$ is the feeding kernel.

The linking activity can be described by:

$$L(t) = G_{Link} e^{-\alpha L \Delta t} L(t-1) + Y(t-1) * M \quad (5)$$

where $G_{Link}$ is the link gain, $\alpha_{L\Delta t}$ is the time constant of the leakage filter of the linking region, and $M$ is the linking kernel.

The internal activity depends on the linking and feeding activity. The internal activity of the neuron is defined as:

$$U(t) = F(t)\left[1 + \beta L(t)\right] \quad (6)$$

where $\beta$ is the linking coefficient and defines the amount of modulation of the feeding due to the linking activity.

The dynamic threshold is implemented by:

$$\theta(t) = e^{-1/\alpha\theta} \theta(t-1) + VY(t) \quad (7)$$

where $\alpha_\theta$ is the time constant of the leakage filter of the threshold and $V$ is the threshold gain.

The output of the neuron is then finally defined by:

$$Y(t) = \begin{cases} 1 & \text{if } U(t) > \theta(t) \\ 0 & \text{otherwise} \end{cases} \quad (8)$$

## 4. RESULTS AND DISCUSSION

Figure 3 shows the results obtained using the PCNN with an original grain image and a blurred version based on the wavelet preprocessing approach presented in Section 2. Twenty iterations are shown starting from the top-left image indexed by 1. Figure 4 shows the same results for another grain image. Note how the borders of the grains obtained using the SWT for the 12th iteration are well defined for both sets of images. Table I summarizes these findings for 5 images indicating that using the SWT and the image obtained at the 12th iteration can be used for automatic segmentation of the grain. Figure 5 shows two more examples at this 12th iteration. Final borders are easily obtained using morphological operations afterwards. Values for the different parameters used in the PCNN are shown in Table II.

## 5. CONCLUSIONS

The authors developed a robust and automatic approach to segment wheat grains from thermal images based on the use of the static wavelet transform and pulse coupled neural networks. Albeit there is considerable overlapping between the gray level ranges of the background and the grains, the use of the wavelet transform helps the neurons of the background and grain pulse together consistently for the 12th iteration using the parameters presented in Table II. Thus, this work suggests that the use of the SWT as a preprocessor to the PCNN can yield accurate segmentations at one particular iteration eliminating any further post-processing to define the right image among the different ones obtained by the PCNN.

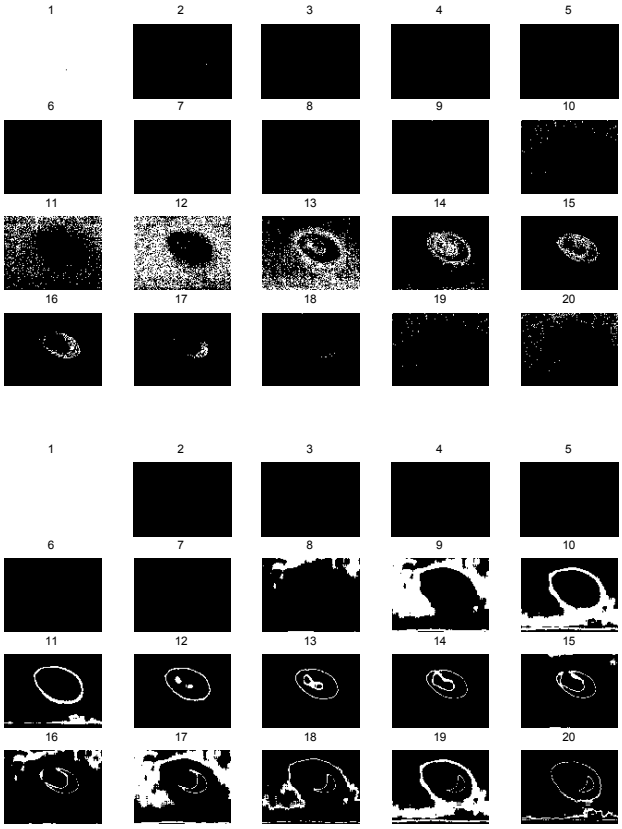


Figure 3. Top: Segmentation using PCNN, no preprocessing. Bottom: Results using the SWT-PCNN segmentation.

Table I

| Image index, method | Number of iterations used | Iteration number for successful segmentation |
|---|---|---|
| 1, original | 20 | 14 |
| 1, wavelet | 20 | 11,12,13 |
| 2, original | 20 | 14 |
| 2, wavelet | 20 | 12,13,14 |
| 3, original | 20 | 13,14 |
| 3, wavelet | 20 | 11,12,13 |
| 4, original | 20 | 13 |
| 4, wavelet | 20 | 11,12 |
| 5, original | 20 | 12,13 |
| 5, wavelet | 20 | 11,12 |

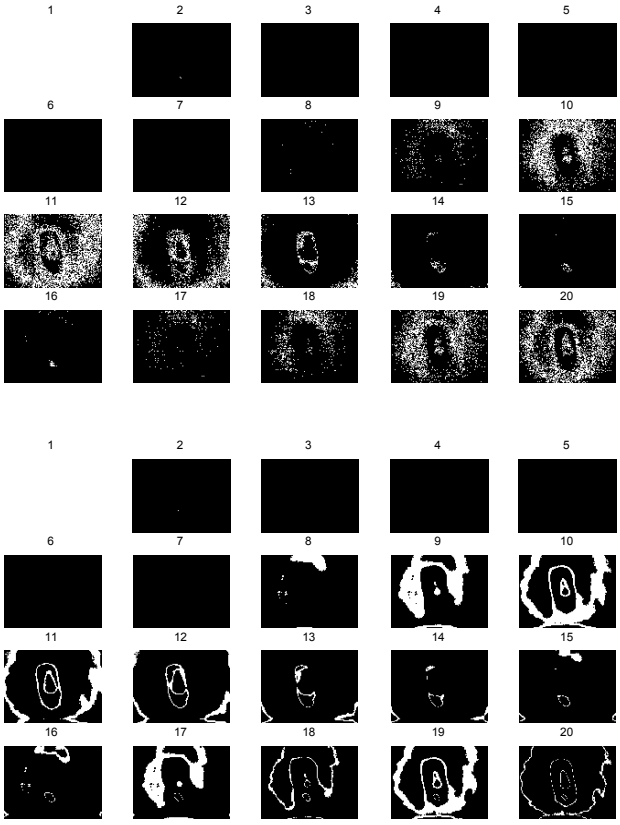


Figure 4. Same as Figure 3 for another grain.

Figure 5. Two more examples of the final SWT-PCNN based segmentation obtained using the image corresponding to the 12th iteration.

Table II

| Parameter | Value |
|---|---|
| Beta | 1 |
| Feed time | -0.1 |
| Feed gain | 0.1 |
| Link time | -0.1 |
| Threshold alpha | 5 |
| Threshold gain | 5 |

## 6. ACNOWLEDGEMENTS

The authors would like to thank the support received from the Natural Sciences and Engineering Research Council of Canada.

## 7. REFERENCES

[1] A. Manickavasagan, *Thermal Imaging for Potential Uses in Cereals and Oilseeds Handling*, Ph.D. Dissertation, University of Manitoba, 2007.

[2] A. Manickavasagan, D.S. Jayas, and D.G. White, "Non-Uniformity of Surface Temperatures of Grain After Microwave Treatment in an Industrial Microwave Dryer," *Drying Technology*, Taylor and Francis, Vol. 24, pp. 1559-1567, 2006.

[3] R. C. Gonzales, and R. E. Woods, *Digital Image Processing*, Second Edition, Prentice Hall, New Jersey, 2002.

[4] M. Sezgin and B. Sankur, "Survey Over Image Thresholding Techniques and Quantitative Performance Evaluation," *SPIE Journal of Electronic Imaging*, Vol. 13, No. 1, pp. 146-168, January 2004.

[5] C. Chui, *Wavelets: A Tutorial in Theory and Applications*, Academic Press, San Diego CA, 1992.

[6] G. Kuntimad and H.S. Ranganath, "Perfect Image Segmentation Using Pulse Coupled Neural Networks," *IEEE Trans. on Neural Networks,* Vol. 10, No. 3, pp. 591–598, May 1999.

[7] J.A. Karvonen, "Baltic Sea Ice SAR Segmentation and Classification Using Modified Pulse Coupled Neural Networks," *IEEE Trans. on Geoscience and Remote Sensing,* Vol. 42, No.7, pp. 1566-1574, July 2004.

[8] Y. Xue and S. X. Yang, "Image Segmentation Using Watershed Transform and Feed Back Pulse Coupled Neural Network," *Artificial Neural Networks: Biological Inspirations*, Springer Berlin / Heidelberg, 2005.

[9] X. Gu and D. Yu, "Image Shadow Removal Using Pulse Coupled Neural Networks," *IEEE Trans. on Neural Networks*, Vol. 16, No. 3, pp. 692-698, May 2005.

[10] W. Li and X. Zhu, "A New Algorithm of Multi-modality Medical Image Fusion Based on Pulse Coupled Neural Networks," *Advances in Natural Computation*, Springer Berlin / Heidelberg, 2005

[11] M. Chacon, S.A. Zimmerman, A.D. Sanchez, "PCNNP: a Pulse-Coupled Neural Network Processor," *International Joint Conference on Neural Networks,* Vol. 2, pp. 1581-1684, May 2002.